Int J Adv Manuf Technol (2015) 77:1005–1017
DOI 10.1007/s00170-014-6535-7

ORIGINAL ARTICLE

Thermal error modeling and compensation for a high-speed motorized spindle

Jun Yang · Hu Shi · Bin Feng · Liang Zhao · Chi Ma · Xuesong Mei

Received: 4 May 2014 / Accepted: 20 October 2014 / Published online: 1 November 2014

Abstract To improve the precision of CNC machine tools, a motorized spindle thermal error model based on least square support vector machine (LS-SVM) was proposed. A thermal error compensation method was implemented, which takes the length of cutting tools and thermal tilt angles into account. A five-point method was applied to measure radial thermal declinations and axial expansion of the spindle with eddy-current sensors. This resolves a problem arising out of the three-point thermal error measurement, where the radial thermal-induced angle errors cannot be obtained. Variables sensitive to thermal error were selected by grouping and optimizing temperature variables using a combined fuzzy cluster and correlation analysis. LS-SVM models were established for axial elongation and radial thermal yaw and pitch angle errors. Moreover, a method to test the goodness of prediction for the results based on the model is discussed. The results indicated that the LS-SVM has high predictive ability based on fuzzy cluster grouping, and prediction accuracy reached up to 90 %. In addition, the axial accuracy was improved by 82.6 % after error compensation, and the axial maximum error decreased from 39 to 8 μm. Moreover, the *X*/*Y* direction accuracy can reach up to 77.4 and 86 %, respectively, which demonstrated that the proposed methodology of measurement, modeling, and compensation was effective.

Keywords Motorized spindle · Thermal tilt angle · LS-SVM · Error compensation · Fuzzy cluster

J. Yang · H. Shi (✉) · B. Feng · L. Zhao · C. Ma · X. Mei
State Key Laboratory for Manufacturing Systems Engineering, Xi'an Jiaotong University, Xi'an 710049, China
e-mail: tigershi@mail.xjtu.edu.cn

1 Introduction

Precision CNC jig boring machines are typically used for processing complex box-type components. Heat generated during the fabrication of these components gives rise to thermal errors. These thermal errors account for a larger proportion of the total error as the machine tools become more sophisticated. As a result, the accuracy of the tool decreases and dimension deviates from the initial design value. This is particularly an issue when the machine is used for longer time periods. One of the factors resulting in the decreased accuracy over time related to usage and machine age is inadequate maintenance of the tool. The reduced accuracy due to the thermal errors accounts for 70 % of the total errors arising from various error sources [1]. Research presented in literature related machine precision such as the one by Donmez et al. also points to temperature variations resulting in manufacturing errors, thereby reducing machine precision [2]. Non-uniform temperature distribution in CNC machine tools varies with time, becoming non-linear and non-stationary. Moreover, the motorized spindles have complex, dynamic, non-stationary, and speed-dependent thermal characteristics in comparison to conventional spindles [3].

In recent years, finite element method (FEM) has been used to analyze temperature distribution and thermal deformation for machine tools. Creighton et al. used FEM to analyze temperature distribution characteristics for a high-speed micro-milling spindle. An exponential model for the axial thermal error was constructed and correlated to spindle speed and run time [4]. Zhao et al. proposed a method to calculate the thermal conductivity coefficient for the spindle surface. Simulations were used to aid in the analysis of the temperature field variation along with thermal deformation of the spindle [5]. However, the tool error for the precision CNC machine tool is a mutually coupled problem with many complex factors, which are in turn governed by numerous variables. This makes it extremely difficult to establish a theoretical equation taking into account thermoelasticity and heat transfer. Yang et al. [6] used artificial neural networks (ANNS) to establish a relationship between temperature of the spindle and the resulting thermal errors. Ouafi et al. constructed an artificial neural network model for spindle thermal error with the temperature drawing on statistical distribution, which effectively improves the machining accuracy [7]. The grey neural network was proposed to predict the thermal error, and experiments on the axial thermal deformation of the spindle in a five-axis machining center are conducted to build and validate the proposed models [8]. Vissiere et al. measured thermal drifts for a spindle with a new method, which allows measurement accuracy with nanometer resolution [9]. Vyroubal et al. focused on compensation methods for the thermal deformation in spindle axis direction, which was based on decomposition analysis. Such a method was found to be low cost in actuality and an effective strategy to reduce the thermal error [10]. Hong et al. studied thermal characteristics of a rotary axis on a five-axis machine and analyzed the relation between thermal and motion error for the rotary axis [11]. Huang et al. proposed a combined thermal error model for the high-speed spindle in a machine tool and used the five-point method to measure the thermal drifts, and a genetic algorithm (GA) was introduced to optimize the BP network's initial weights and thresholds, solving the global minimum searching problem [12].

In addition, the temperature sensor selection for the thermal error modeling of the machine tool is important. The fuzzy c-means clustering method and the ISODATA method are used to group the data of thermal sensors, which are effective for thermal sensor selection [13]. The direct criterion method and indirect grouping method based on the synthetic grey correlation theory were presented to optimize the selection of a minimum number of temperature sensors for thermal error compensation on a machine tool. After optimization, the number of thermal points reduced from 16 to 4 [14].

If thermal errors propagate through the measurement and modeling stage, they can be alleviated by employing compensation methods. Zhang et al. proposed one such compensation technique to improve machine precision, which is based on the use of the external machine zero point shift function. Ethernet data communication protocol was used for the machine tools [15]. Fu and Miao et al. built the spindle axial thermal error model using a multivariate linear regression method [16, 17]. The use of axial thermal error compensation method as a method for improving the machine precision has also been reported in literature by other research groups [18, 19]. Pajor et al. presented a method for supervising the feed screw thermal elongation. This method reduced ball screw thermal errors [20]. Wu et al. has successfully achieved real-time compensation for axial expansion on a vertical machine tool by using a multiple regression model [18]. Liu et al. compensated the thermal drift of milling and boring machines along the Z direction [21]. Ouafi et al. presented an integrated and comprehensive modeling approach for real-time thermal error compensation based on multiple temperature measurements. After the use of this compensation strategy, spindle errors were reduced from 19 μm to less than 1 μm [7]. Gebhardt et al. described a high-precision grey box model for compensating thermal errors for a five-axis machine. Using this method, the thermal errors for rotation/swiveling were reduced by a factor of 85 % [22]. Wang et al. proposed another prediction model for axial thermal deformation and applied the model to compensate the error for a CNC machine [23].

The methods reported in literature mainly discuss measurement and modeling methods for spindle axial thermal elongation. However, the existing methods fail to take into account errors resulting from the radial thermal angle error. Spindle thermal deformation for a CNC machine tool is usually expressed as deviation from the spatial position and gestures, i.e., the drift in geometry and spatial phase, which affects machining precision. Here, we consider the jig boring machine, particularly the thermal expansion of the spindle axial of the tool, which affects the geometry of the bore. In addition, errors due to the radial thermal angle could affect the geometry and surface roughness of the bore. Due to this, it is critical to measure both axial and radial thermal errors simultaneously. To realize error compensation, the error due to the spindle radial thermal angle must be translated to the linear coordinate axis. The compensated components of the thermal errors are closely related to spindle radial thermal inclination angle errors and handle length. Using a three-point method, the absolute thermal deformation along a radial direction can be measured and it does not reflect the variations in radial thermal deformation for the spindle. The thermal inclination angle errors cannot be obtained using this method and results in a thermal error compensation model with reduced accuracy.

To improve the accuracy and overcome the disadvantages associated with the three-point method, a five-point method is proposed. In comparison to other methods, the five-point method has the advantage of allowing simultaneous measurement of axial and radial thermal drifts for the motorized spindle system. As a result, the variation in the spindle position and orientation can be analyzed. This overcomes the challenge in measurement of inclined angles for the spindle radial thermal errors often associated with the three-point method. Moreover, an integrated thermal error model provides a more accurate mathematical model for the thermal error compensation, which includes spindle thermal elongation, radial thermal pitch angle error, and yaw angle errors based on the five-point method.

The support vector machine is a new machine learning theory, which has the advantage of using a simple and versatile algorithm. It depends on using training data with good generalization and global optimization characteristics, which can be used for parameters with non-linear relationships. Lin and Zhao et al. [24, 25] established a spindle thermal error model based on the least square support vector machine theory. This model was found to have perfect robustness. However, as in the previous cases, their model also ignored radial declination angle errors.

To the best of our knowledge, a method based on the least square support vector machine and fuzzy clustering to model thermal elongation and declination angles has not been presented in current literature. The proposed model can be used to predict axial and radial errors with high accuracy. Thermal drifts using this method were translated into coordinate offsets and were used to establish mathematical equations for final compensation along three directions, allowing improvement in the machine tool accuracy.

The current study focuses on a spindle system, which is used in a box-type precision CNC jig boring machine. Thermal balance experiments were performed using the five-point method. Least square support vector machine (LS-SVM) models are established for spindle axial thermal elongation and radial thermal declinations, using the fuzzy clustering regression analysis method to optimize the temperature variables. Subsequently, thermal error offset equations were derived and the compensation was carried out.

2 Thermal error modeling

2.1 Hierarchical clustering method to group temperature variables

A variety of fuzzy clustering analysis methods based on the fuzzy graph theory have been proposed in literature. Among them, the biggest tree method based on the fuzzy graph theory is the most popular [26]. The fuzzy c-means clustering method is applied to identify the temperatures, and the representative as an independent variable is selected; meanwhile, it eliminates coupling among the variables [27]. In this paper, temperature variables for 11 measuring points were grouped using fuzzy clustering. Statistical correlation was then applied to optimize the measurement points. The correlation coefficient between each variable temperature and thermal error were calculated. Finally, the measurement points with the largest value for the correlation coefficient in each group were taken as the typical temperature variables. The number of variables for temperature is small, so system cluster analysis was used. The variable packet flows are shown in Fig. 1.

Assume the temperature variable $T=\{T_1, T_2,\ldots, T_m\}$ is the object carried out using fuzzy clustering analysis. Each object in T is denoted as T_k ($k=1, 2,\ldots, m$), whose characteristics are described by finite values. A corresponding vector $P(T_k)=(T_{k1}, T_{k2},\ldots, T_{ks})$ is related to T_k. T_{kj}($j=1, 2,\ldots, s$) is the jth characteristics value of T_k. $P(T_k)$ is the eigenvector for T_k. Fuzzy clustering analysis divides the sample T into c fuzzy subsets $\widetilde{T}_1, \widetilde{T}_2, \ldots, \widetilde{T}_c$, according to the similarity between the feature vectors.

Cluster analysis, also known as hierarchical clustering analysis, gradually clusters based on feature vector distance criteria. The classification moves from more to less, until it reaches the desired classification. The following are the general steps used for system clustering:

1. Initialize data, assuming that the sample set T contains m subsets $T_1^{(0)}, T_2^{(0)},\ldots, T_m^{(0)}$, which form one class. Then, distance is calculated between each subset to obtain a $m\times m$ dimensional distance matrix $D^{(b)}$.
2. Next, the smallest element in the distance matrix $D^{(b)}$ (except diagonal elements) is determined. If the minimum element is the distance between $T_i^{(b)}$ and $T_j^{(b)}$, then the two elements are merged into $T_{ij}^{(b+1)}$. Finally, a new classification $T_1^{(b+1)}, T_2^{(b+1)},\ldots, T_{m-1}^{(b+1)}$ is obtained.
3. After this, distances between the new categories after obtaining merging cluster to get the distance matrix $D^{(b+1)}$.
4. Step 2 is repeated until the classification meets the requirements.

2.2 Least square support vector machine

The support vector machine (SVM) is an approach based on statistical leaning and minimized structural risk. Vapnik [28] suggested that it is dependent on training data to a small degree with good generalization and global optimization characteristic and can be used to handle parameters with non-linear relationship. Suykens et al. proposed a modification by using a sum of squared error terms in the standard SVM objective function. This new sum was used as the loss function. The new method is referred to as the least square (LS)-SVM [29].

The modeling process for LS-SVM, which is used to solve the problem, is described as [29]

$$\min J(\omega,\xi_i)=\frac{1}{2}\|\omega\|^2+\gamma\frac{1}{2}\sum_{i=1}^{l}\xi_i^2$$
$$\text{s.t. } y_i=\omega^T\varphi(x_i)+b+\xi_i \quad i=1,\ldots,l \tag{1}$$

where J is the function with structural minimized risk, and ω is a weight vector, $\omega\in R^n$. ξ_i is the error variable, and γ is an adjustable parameter. x_i is the input, $x_i\in R^n$. y_i is the target volume. $\varphi(\cdot)$ is a mapping function, where a low-dimensional space can be mapped to the n-dimensional kernel space. b is the deviation, and l is the number of inputs.

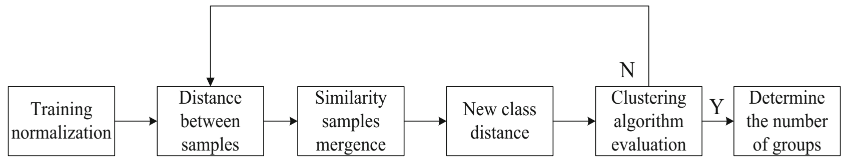

Fig. 1 Fuzzy clustering grouping

To build the Lagrange function using Eq. (1),

$$L(\omega,\xi_i,b,\alpha_i)=\frac{1}{2}\|\omega\|^2+\gamma\frac{1}{2}\sum_{i=1}^{l}\xi_i^2-\sum_{i=1}^{l}\alpha_i\left(\omega^T\varphi(x_i)+b+\xi_i-y_i\right) \tag{2}$$

where the parameter $\alpha_i(i=1,\cdots,l)$ is a Lagrange multiplier. Based on the necessary conditions for extreme value, the following equations can be induced:

$$\begin{cases}\dfrac{\partial L}{\partial\omega}=0\Rightarrow\omega=\displaystyle\sum_{i=1}^{l}\alpha_i\varphi(x_i)\\ \dfrac{\partial L}{\partial\xi_i}=0\Rightarrow\alpha_i=\gamma\xi_i\\ \dfrac{\partial L}{\partial b}=0\Rightarrow\displaystyle\sum_{i=1}^{l}\alpha_i=0\\ \dfrac{\partial L}{\partial\alpha_i}=0\Rightarrow y_i=\omega^T\varphi(x_i)+b+\xi_i\end{cases} \tag{3}$$

and $i=1,\cdots,l$; then, ω and ξ_i are eliminated from Eq. (3), and the matrix equation can be obtained.

$$\begin{pmatrix}0 & 1 & \cdots & 1\\ 1 & K(x_1,x_1)+1/\gamma & \cdots & K(x_1,x_l)\\ \vdots & \vdots & & \vdots\\ 1 & K(x_l,x_1) & \cdots & K(x_l,x_l)+1/\gamma\end{pmatrix}\begin{pmatrix}b\\ \alpha_1\\ \vdots\\ \alpha_l\end{pmatrix}=\begin{pmatrix}0\\ y_1\\ \vdots\\ y_l\end{pmatrix} \tag{4}$$

According to Mercer conditions [22], the LS-SVM regression analytic formula can be induced by applying the kernel function $K(x,x_i)$.

$$f(x)=\sum_{i=1}^{l}\alpha_iK(x,x_i)+b \tag{5}$$

In Eq. (5), α_i and b are calculated using Eq. (4). The kernel function $K(x_i,x_j)$ is any symmetric function which satisfies the Mercer conditions. Here, the radial basis function (RBF) is chosen as the kernel function and is given by

$$K\left(x_i,x_j\right)=\exp\left(-\frac{\left\|x_i-x_j\right\|^2}{2\sigma^2}\right) \tag{6}$$

3 Spindle thermal characterization experiment

3.1 Experimental setup

The experimental system is shown in Fig. 2, which shows the spindle of a precision CNC jig boring machine. A synchronous acquisition system was used for measurements and to determine the temperature along with the associated thermal deformation. This system uses *Pt*100 precision magnetic temperature sensors to measure temperature for the spindle system. High-precision eddy-current sensors were used to measure thermal drifts in the spindle. Temperature sensors were located on front bearing (T_6, T_7), rear bearing (T_1), motor (T_8, T_{11}), ambient temperature (T_5), spindle base (T_2), the cooling fluid inlet (T_9), bearing cooling out (T_3), front bearing coolant out (T_4), and the motor cooling out (T_{10}).

3.2 Measurement principle

The spindle thermal drifts were measured using a five-point method [30]. A displacement sensor measurement setup is shown in Fig. 3. The spindle is parallel to the *Z*-axis, and the axial thermal expansion can be obtained by S_5. Radial thermal yaw θ_x along the partial *X* direction was measured by sensors S_1 and S_3, whereas radial thermal pitch θ_y along the partial *Y* direction was measured using sensors S_2 and S_4.

After the spindle was run for long time periods, thermal expansions occur along the axial direction and thermal angle inclination occurs along the radial direction. This results from the uneven temperature gradient distribution, which is shown in Fig. 4, and the thermal yaw angle is

$$\Delta L_3=L_3^i-L_3^0 \tag{7}$$

$$\Delta L_1=L_1^i-L_1^0 \tag{8}$$

$$\Delta L=\Delta L_3-\Delta L_1 \tag{9}$$

$$\tan\theta_x=\frac{\Delta L}{D_s} \tag{10}$$

where i denotes the number of measurements. The thermal yaw angle is negligible for this experiment, that is

Fig. 2 Experimental setup showing the spindle of a precision CNC jig boring machine

$\theta_x \rightarrow 0$, so:

$$\theta_x \tilde{} \tan\theta_x \tag{11}$$

As shown in Eq. (12), the thermal yaw can be obtained by applying Eqs. (7)–(11).

$$\theta_x = \frac{\left(L_3^i - L_1^i\right) - \left(L_3^0 - L_1^0\right)}{D_s} \tag{12}$$

where L_3^0 and L_1^0 are the radial displacement between the sensor probe and the spindle measured by S_3 and S_1, respectively. L_3^i and L_1^i are the transient displacement during operation. D_s is the distance between S_1 and S_3 and S_2 and S_4, and D_s=120 mm.

Similarly, the thermal pitch angle in the Y direction can be obtained:

$$\theta_y = \frac{\left(L_4^i - L_2^i\right) - \left(L_4^0 - L_2^0\right)}{D_\mathrm{s}} \tag{13}$$

3.3 Results and analysis

The spindle speed affects the temperature field distribution and the magnitude of thermal drifts. In order to simulate actual spindle speed during processing, the specific speed distribution is shown in Fig. 5.

The spindle system temperature variation is shown in Fig. 6. The overall trend for the temperatures at all the measuring points increases with time. In general, a cyclical change in temperature was observed with time. This is because the temperature of the spindle system was controlled by an intelligent cooling system, which sets a temperature threshold value and starts to reduce the temperature when the component temperature exceeds the threshold value. Therefore, the increase in temperature exhibits fluctuations. The rear bearing had the highest temperature at 30.4 °C. This occurs due to its large capacity, heavy load, and severe friction, which generates more heat. The next component with the highest temperature was the motor with a temperature of 26.7 °C.

The measurements shown in Fig. 7 indicate that the displacement trends gradually increase over time, eventually reaching thermal equilibrium. Z-axis axial thermal elongation increases with time. The elongation direction is negative, which indicates spindle thermal expansion to the negative direction on the Z-axis. It takes approximately 385 min to reach thermal equilibrium, and the maximum elongation was 39.6 μm. Thermal error on X-axis direction is positive, which indicates that during the heating process, the spindle is away from the displacement sensors S_1/S_3. It deviates from the Z-axis, and the spindle swings to the negative direction along the X-axis on the XZ plane. Thermal yaw angle to the Z-axis in this case is θ_x, and the maximum heat offset error was 35.8 μm. Thermal error in the Y direction is negative, which indicates that during operation the spindle is closer to the displacement sensors S_2/S_4. It deviates from the Z-axis, and the spindle in the YZ plane pitches to the negative direction on the Y-axis. The thermal pitch angle to the Z-axis in this case is θ_y, and the maximum thermal offset was 20.2 μm.

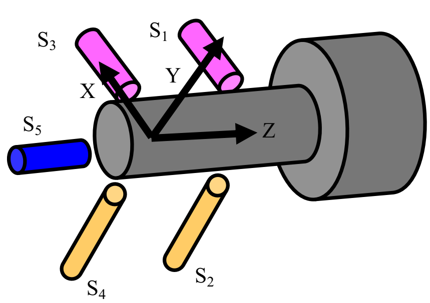

Fig. 3 Spindle five-spot installation diagram

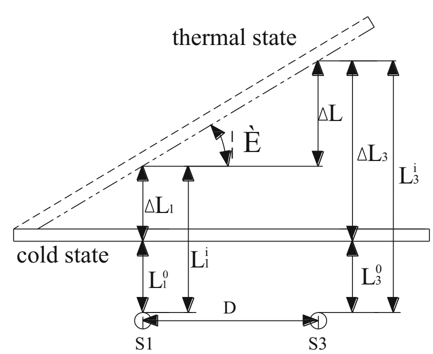

Fig. 4 The spindle thermal inclination sketch

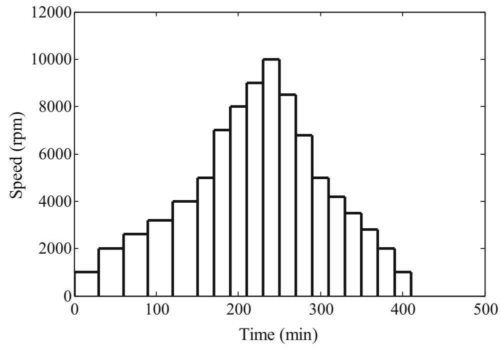

Fig. 5 Step speeds distribution

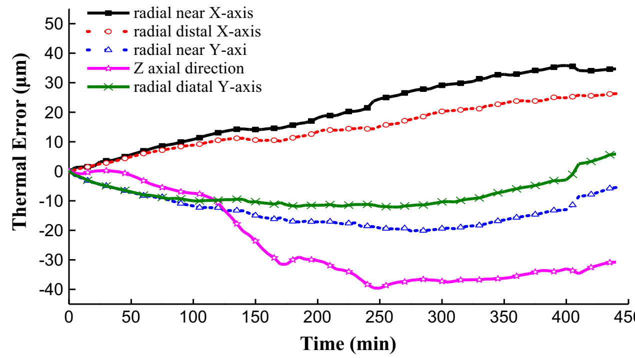

Fig. 7 Thermal drifts for the spindle

4 Thermal error prediction and compensation

4.1 Parameter identification and model training

Optimization of thermal key points, m=11, sets the number of packets C=4, after calculating, and the combination of Euclidean-centroid clustering algorithm obtained the optimal grouping; the cluster groupings shown in Fig. 8 divide the temperature variables into groups $\{T_1\}$, $\{T_5\}$, $\{T_2, T_3, T_4, T_6, T_9, T_{10}\}$, and $\{T_7, T_8, T_{11}\}$.

Based on the results for the groups, correlation coefficients between axial thermal error E and the temperature T_i can be calculated as follows:

$$\rho_{T_iE} = \frac{\sum_{j=1}^{n}\left(T_{ij}-\overline{T}_i\right)\left(E_j-\overline{E}_j\right)}{\sqrt{\sum_{j=1}^{n}\left(T_{ij}-\overline{T}_i\right)^2}\sqrt{\sum_{j=1}^{n}\left(E_j-\overline{E}_j\right)^2}} \tag{14}$$

In the above equation, i= 1, 2,…, m refers to the temperature measurement points and j= 1, 2,…, n refers to the number of measurements. T_{ij} is the temperature of the measuring point, E_j is the thermal elongation, $\overline{T}_i$ is the average temperature of the ith measurement point, and $\overline{E}_j$ is the average thermal elongation. Correlation coefficients are listed in Table 1. The temperature variable with the highest coefficient was selected as a typical variable in each cluster. T_{10} is the outlet liquid temperature of the motor coolant, and its temperature has a significant influence on motor temperature. Thus, T_{10} is reserved as a key variable. Finally, T_1, T_5, T_6, T_7, and T_{10} were chosen as the typical temperature variables.

Using the five identified temperature variables as the input, namely x=[T_1, T_5, T_6, T_7, T_{10}], and x_j=[T^j_1, T^j_5, T^j_6, T^j_7, T^j_{10}] as temperature vector of the jth measurement, j=1,⋯,l and l=89. Lagrange coefficients of thermal elongation E, thermal yaw angle θ_x, and thermal pitch angle θ_y are α_i,β_i,η_i, respectively, and the corresponding deviations are b_1,b_2,b_3. Then, the ranges of values are:

$$\begin{cases} \gamma_n = 5n, \quad n = 1, 2, \cdots, 20, \quad \text{and} \quad \gamma_0 = 1 \\ \sigma_k^2 = 1 + 0.5k, \quad k = 0, 1, \cdots, 18 \end{cases} \tag{15}$$

Through the use of the cross-validation method (CV) for solving γ and σ, Lagrange coefficients α_i,β_i,η_i and deviation b_1,b_2,b_3 were calculated by Eqs. (4) and (6). Shown in Table 2, the LS-SVM consists of 89 vector machines.

4.2 Model prediction

The sample size for the data is 89. LS-SVM is used to predict thermal drifts for the spindle. The curve fitting and actual measurements are compared in Figs. 9, 10, and 11.

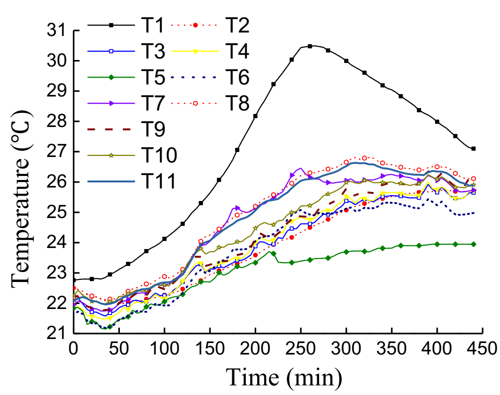

Fig. 6 Temperatures of the spindle

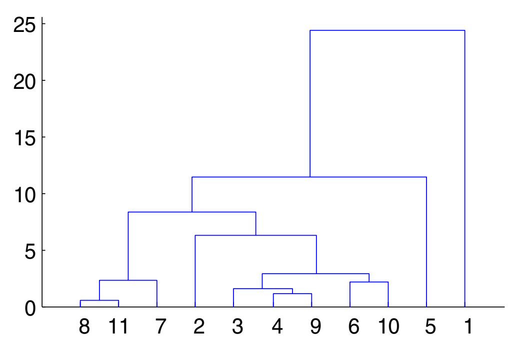

Fig. 8 Clustering dendrogram

Table 1 Correlation coefficients between temperature and axial thermal error

Temperature	T_1	T_2	T_3	T_4	T_5	T_6	T_7	T_8	T_9	T_{10}	T_{11}
Cluster T	4	2	2	2	3	2	1	1	2	2	1
ρ	0.9651	0.8593	0.9054	0.9242	0.9546	0.9706	0.9902	0.9739	0.8948	0.9344	0.9737

The evaluation criteria for fitting the model need to be established, assuming the absolute value of the residual error is $|e_i|$, minimum as $|e_i|_{\min}$, maximum as $|e_i|_{\max}$, and mean values as $\overline{|e_i|}$. Root mean square error is RMSE, the determination coefficient is R^2, and the predictive ability is η.

$$\mathrm{RMSE} = \sqrt{\frac{\sum_{i=1}^{n}\left(y_i - \widetilde{y}_i\right)^2}{n}} \tag{16}$$

$$R^2 = 1 - \frac{\sum_{i=1}^{n}\left(y_i - \widetilde{y}_i\right)^2}{\sum_{i=1}^{n}\left(y_i - \overline{y}_i\right)^2} \tag{17}$$

$$\eta = 1 - \frac{\frac{1}{n}\sum_{i=1}^{n}\left|y_i - \widetilde{y}_i\right|}{\frac{1}{n}\sum_{i=1}^{n}|y_i|} = 1 - \frac{\sum_{i=1}^{n}\left|y_i - \widetilde{y}_i\right|}{\sum_{i=1}^{n}|y_i|} \tag{18}$$

where y_i is the measurement value, $_i$ is the predicted value by the thermal error model, $\overline{y}_i$ is the average value of the measurement, i=1,⋯,n, and n is the number of data points. The fitting performance parameters of the least square support vector machine are shown in Table 3.

The absolute mean value of the residual error is small, the RMSE are close to zero, and the coefficient of determination R^2 is close to 1. In addition, the predictive ability of the model in the three different directions was more than 90 %, which indicates that the LS-SVM model has higher prediction accuracy.

Table 2 The parameters for LS-SVM

Output	γ	σ^2	b	l
E	50	1	0.2390	89
θ_x	5	2	0.1930	89
θ_y	75	8	−0.1217	89

4.3 Thermal error compensation

4.3.1 Compensation equation of thermal drifts

Figure 12 describes the spatial pose of the spindle thermal drift on XOZ, and the point P is the deflexion center. Through axial elongation E and radial inclination θ_x, the spindle declined from $\overrightarrow{PO}$ to $\overrightarrow{PO'}$, so the thermal offset component in the X direction can be written as

$$\Delta O_x = (D_{0x} + D_t + \Delta D)\sin\theta_x \tag{19}$$

where the offset in the X direction is ΔO_x, D_{0x} is the distance between deflexion center and spindle nose, D_t is the length of the tool, and ΔD is the axial elongation E.

The thermal offset in the Z direction is ΔO_z:

$$\Delta O_z = \Delta D - \Delta O_D = \Delta D - (D_{0x} + D_t + \Delta D)(1 - \cos\theta_x) \tag{20}$$

Because the axial elongation is less than the length of the tool, that is

$$\Delta D << D_{0x} + D, \quad \text{and} \quad \theta_x \rightarrow 0 \tag{21}$$

so

$$\begin{aligned} \sin\theta_x &\rightarrow \theta_x \\ \cos\theta_x &\rightarrow 1 \end{aligned} \tag{22}$$

Equations (21) and (22) were substituted into Eqs. (19)–(20), then thermal offsets in the X and Z directions can be obtained.

$$\Delta O_x = (D_{0x} + D_t)\theta_x \tag{23}$$

$$\Delta O_z = \Delta D \tag{24}$$

This indicates that the thermal offset in the Z direction has no relationship with the tool length, while the X directional thermal offset is closely related to the tool length.

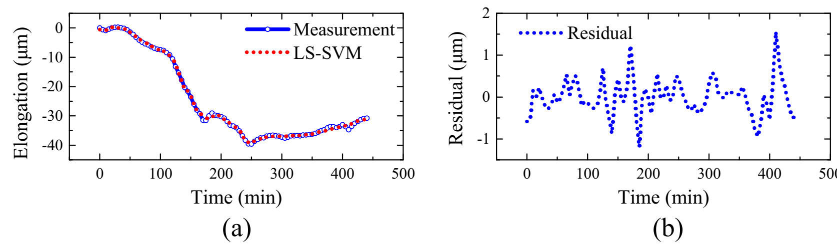

Fig. 9 Axial thermal elongation: **a** the prediction and measurement; **b** residual error

Similarly, the thermal error offset ΔO_y in the Y direction can be obtained:

$$\Delta O_y = \left(D_{0y} + D_t\right)\theta_y \tag{25}$$

where D_{0y} is the distance between the deflexion center and spindle nose.

Assuming the distance between the deflexion center and spindle nose is D_{0x}, D_{0y} in the X and Y directions, respectively, as is shown in Fig. 12b, there is

$$D_{0x} = \frac{\Delta L_1}{\tan\theta_x} - D_{L1} = 548.659 \text{ mm} \tag{26}$$

$$D_{0y} = \frac{\Delta L_2}{\tan\theta_y} - D_{L2} = 508.706 \text{ mm} \tag{27}$$

In Eq. (26), $\Delta L_1 = L_1^i - L_1^0$ and the value is measured by the displacement sensor S_1, which is shown in Fig. 7. $\tan\theta_x \sim \theta_x$, the θ_x is shown in Fig. 10a calculated by Eq. (12). ΔL_1 and θ_x are dynamic changed state variables, and the ratio of them is also dynamic changed, but the fluctuation is small and the ratio is close to 791.817 mm, so treat $\frac{\Delta L_1}{\tan\theta_x} = 791.817$ mm . In a similar way, in Eq. (27), $\Delta L_2 = L_2^i - L_2^0$ and the value is acquired by the displacement sensor S_2, which is also shown in Fig. 7. The computed result of θ_y is shown in Fig. 11a, and treat $\frac{\Delta L_1}{\tan\theta_x} = 751.864$ mm .

The distance between displacement sensors S_1, S_2 and the spindle nose is D_{L1},D_{L2}, and D_{L1}=D_{L2}=243.158 mm.The thermal offsets for the coordinate can be obtained by applying Eqs. (5) and (23)–(27).

$$\Delta O_x = (D_t + 548.66)\left[b_2 + \sum_{i=1}^{l} \beta_i K(x, x_i)\right] \tag{28}$$

$$\Delta O_y = (D_t + 508.71)\left[b_3 + \sum_{i=1}^{l} \eta_i K(x, x_i)\right] \tag{29}$$

$$\Delta O_z = b_1 + \sum_{i=1}^{l} \alpha_i K(x, x_i) \tag{30}$$

where $x=[T_1, T_5, T_6, T_7, T_{10}]$, $\alpha_i, \beta_i, \eta_i$, and b_1, b_2, b_3 are as shown in Table 2.

4.3.2 The principle of thermal error compensation

The motorized spindle system of the precision jig boring machine deflects its ideal position space because of the thermal error, and it can be learned that the thermal offsets on the three directions are all negative through experimental analysis, as shown in Figs. 9a, 10a, and 11a. Define the thermal deviation vector of the cutting tool as $\overrightarrow{OO'}$:

$$\overrightarrow{OO'} = \left\{-\Delta O_x, -\Delta O_y, -\Delta O_z\right\} \tag{31}$$

The accuracy of the machine tool is determined by the relative displacement between the cutter and workpiece in machining. Based on the analysis of Eq. (31), the thermal error leads the spindle system to generate thermal offsets on three coordinate directions and reduces the machining

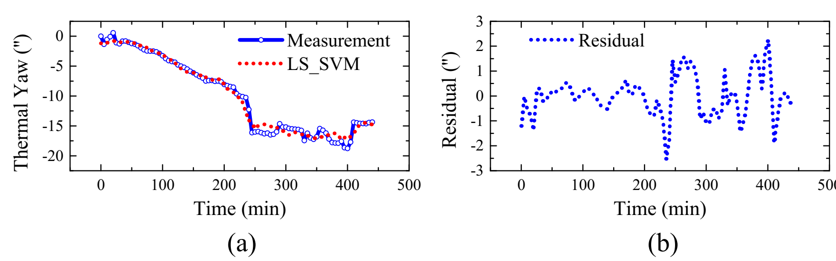

Fig. 10 Radial thermal yaw angle: **a** the prediction and measurement; **b** residual error

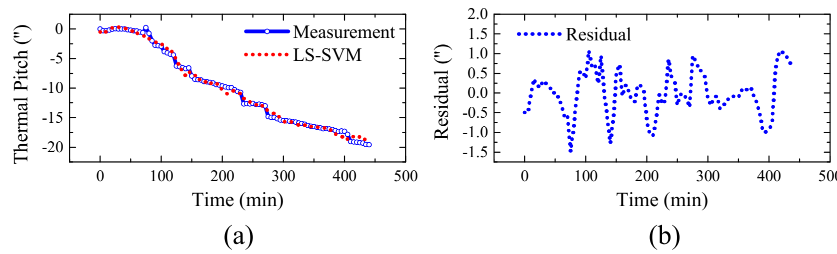

Fig. 11 Radial thermal pitch angle: **a** the prediction and measurement; **b** residual error

accuracy. In order to eliminate the impact of the thermal offsets, the extra compensated amount must be added on the coordinate of the workpiece, so the essence of the thermal error compensation is to move the kinematic pair of the machine tool to make the cutter and the workpiece generate a relative motion in the opposite direction of the machine tool thermal offset, and compensates the error resulting from the thermal deformation. As shown in Fig. 13, the compensation signal of the thermal error is inserted into the CNC system and superimposed with the machining coordinate values and the feedback signal of the encoder. Then, the new synthetic coordinates are utilized to control the machine tool motion, thus realizing the final compensation of the thermal errors.

In order to improve the machining accuracy, eliminating the effect of thermal drifts on the spindle, the direction of the thermal error compensation component is opposite to the tool thermal offsets vector, and the amount of them should be equal:

$$\Delta H_s = -\overrightarrow{OO'} \tag{32}$$

where ΔH_s is the final compensation vector of the spindle system thermal errors.

Assuming that $OW(P_x, P_y, P_z)$ is the coordinate of a point W on the workpiece, after conducting the thermal error compensation, the new coordinates of the point W becomes $OW'(P_x', P_y', P_z')$, and satisfies

$$OW' = OW + \Delta H_s \tag{33}$$

Substitute Eqs. (31) and (32) into Eq. (33):

$$\begin{cases} P_x' = P_x + (D_{ox} + D_t)\theta_x \\ P_y' = P_y + (D_{0y} + D_t)\theta_y \\ P_z' = P_z + E \end{cases} \tag{34}$$

Table 3 The fitting performance parameters for LS-SVM

Output	$\|e_i\|_{\min}$ µm	$\|e_i\|_{\max}$ µm	$\overline{\|e_i\|}$ µm	RMSE	R^2	η %
E	0.002	1.556	0.313	0.427	0.999	98.7
θ_x	0.008	2.552	0.645	0.846	0.980	93.6
θ_y	0.002	1.489	0.447	0.565	0.992	95.6

The mathematical models of the axial thermal elongation E, the radial thermal yaw angle error θ_x, and the thermal pitch angle error θ_y have been established in Section 4.2, substituting these prediction models into Eq. (34) to get the final coordinates of the workpiece, and the new coordinates being compensated are as follows:

$$\begin{cases} P_x' = P_x + \Delta O_x = P_x + (D_t + 548.66)\left[b_2 + \sum_{i=1}^{l} \beta_i K(x, x_i)\right] \\ P_y' = P_y + \Delta O_y = P_y + (D_t + 508.71)\left[b_3 + \sum_{i=1}^{l} \eta_i K(x, x_i)\right] \\ P_z' = P_z + \Delta O_z = P_z + b_1 + \sum_{i=1}^{l} \alpha_i K(x, x_i) \end{cases} \tag{35}$$

The compensation components of the thermal errors on three coordinate axes are

$$\Delta H_s = \begin{pmatrix} \Delta x \\ \Delta y \\ \Delta z \end{pmatrix} = \begin{pmatrix} (D_t + 548.66)\left[b_2 + \sum_{i=1}^{l} \beta_i K(x, x_i)\right] \\ (D_t + 508.71)\left[b_3 + \sum_{i=1}^{l} \eta_i K(x, x_i)\right] K(x, x_i) \\ b_1 + \sum_{i=1}^{l} \alpha_i \end{pmatrix} \tag{36}$$

where D_t is the length of the cutting tools, $\Delta x, \Delta y, \Delta z$ are the compensation values in the X, Y, and Z directions, respectively, and they are compensated by the CNC controller.

Figure 13 is a schematic diagram of the setup for the spindle thermal error compensation. The Siemens 840D CNC system is used for the experiment. The temperature module acquires signal from PT100 and sends them to the CNC system using RS-232 communication. A thermal error compensation module is embedded into CNC based on secondary development of 840D. It can receive error compensation parameters and then passes them on to the PLC. Finally, thermal error offset was calculated and sent to the CNC to achieve compensation using PLC. While the thermal yaw error and pitch error were translated into the components of

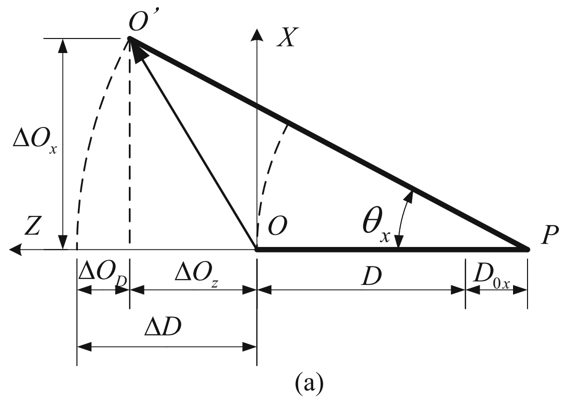

Fig. 12 The geometric principle of the spindle thermal error compensation

the coordinate axis, three components were compensated by the principle described of this compensation system.

4.3.3 Results and comparison

In order to compare with the compensation effect of the five-point method, the compensation algorithm based on the three-point method is established. There are two displacement sensors in the radial direction based on the three-point method, but each of the radial planes has only one sensor. As shown in Fig. 12b, it has only one sensor, S_3 or S_1, in the XOZ plane. The end of the spindle is the point O and S_3 is closer to it, and the measured thermal yaw angle error is larger and the compensation effect is better than S_1, so the measured data of S_3 is chosen to build the compensated model and compared with the five-point method. In the cool state, sign the measured point of S_3 on the spindle as N. When the spindle is at the thermal state, the point is H. In order to verify the effect of the thermal error compensation, it is needed to compare the measured values of S_3 before/after compensation.

Before the compensation, the measured thermal yaw angle error was $\overrightarrow{NH}$:

$$\overrightarrow{NH} = \Delta L_3 = L_3^i - L_3^0 \qquad (37)$$

For the motorized spindle system, the thermal offsets of the end of the tool are compensated by the CNC system, that is, the compensation values of the thermal errors are added to the coordinates of the tool end point O'. Before compensation, the thermal offset of S_3 is the measured value $\overrightarrow{NH}$, and the three-point method treats $\overrightarrow{NH}$ as the compensation component in the X direction, which means that the CNC system compensates $\overrightarrow{NH}$ at the point O'. But the actual distribution value at

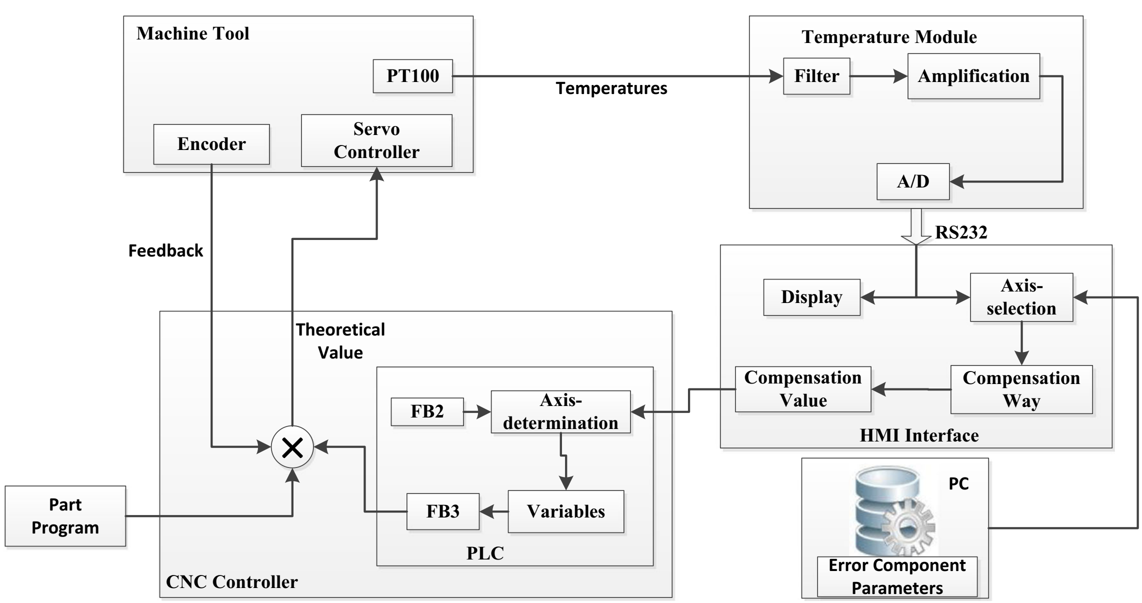

Fig. 13 Thermal error compensation control

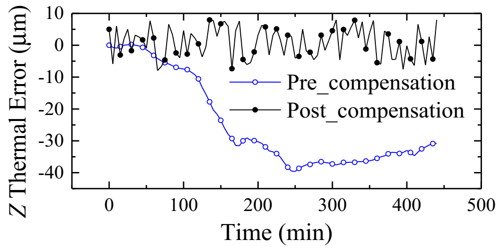

Fig. 14 Axial thermal elongation compensation in the Z direction

point H of the compensation value is $\vec{NH_3}$. For $\Delta O'MP \cong \Delta HNP$, so there is the following proportional:

$$\frac{\vec{NH_3}}{\vec{O'M}} = \frac{D_{ox}+D_{L1}+D_s}{D_{ox}+D_t+\Delta O_z} \tag{38}$$

The actual compensated component of the thermal yaw angle error at point O' is $\vec{NH}$ based on the three-point method, that is:

$$\vec{O'M} \sim \vec{NH} \tag{39}$$

Applying the three-point method, the actual compensation value of the measured point H at the spindle is $\vec{NH_3}$. It can be obtained by applying Eqs. (38) and (39):

$$\vec{NH_3} = \frac{D_{ox}+D_{L1}+D_s}{D_{ox}+D_t+\Delta O_z}\vec{NH} \tag{40}$$

Equation (40) illustrates that, before compensation, the measurement $\vec{NH}$ decreases with the increase in the distance between the measuring point N of S_3 with the spindle end; the compensated value could reduce and the compensation effect may become bad.

While the actual compensated component of the thermal yaw angle error at point O' is $\vec{O'M}$ based on the five-point method, that is:

$$\vec{O'M} = \Delta O_x = (D_{ox}+D_t)\theta_x \tag{41}$$

The actual compensation value of the measured point H at the spindle is $\vec{NH_5}$. It can be induced by Eq. (41):

$$\vec{NH_5} = \frac{D_{ox}+D_{L1}+D_s}{D_{ox}+D_t+\Delta O_z}(D_{ox}+D_t)\theta_x \tag{42}$$

It is obvious that

$$\vec{NH_3} < \left(\vec{NH} \approx \vec{NH_5}\right) \tag{43}$$

The compensation principle of the thermal pitch angle error on the YOZ plane and the measured values of S_4 before/after compensation are compared.

The spindle system moves in the opposite directions of the thermal offsets when the compensation is carried out. Therefore, the measurement of the displacement sensor S_3 will decrease after compensation; the more it decreases, the more the compensated amount is, and the better the compensation effect is. Inequality (43) presents that the compensated amount in the five-point method is larger than that of the three-point method, which is closer to the measurement $\vec{NH}$ before compensation, and its compensation effect is better than that of the three-point method.

After the compensation for thermal error, the errors in axial and radial directions reduced significantly and are shown in Figs. 14, 15, and 16. Applying the five-point method, the axial maximum error decreased from 39 to 8 μm, and the average error reduced from 24.6 to 4.3 μm, namely the average offset is about 20 μm. Axial accuracy improved by 82.6 %, which demonstrates that the method based on the proposed measurement and modeling is effective. The absolute average value of radial X direction thermal error S_3 reduced from 14.6 to 4.9 μm, and accuracy improved by 66 %. Meanwhile, the absolute maximum value of radial Y direction thermal error S_4 reduced from 12.1 into 2.3 μm with accuracy improving by 90 %, while the axial and radial accuracy were improved by 82.6, 43, and 30.6 %, respectively, based on the three-point

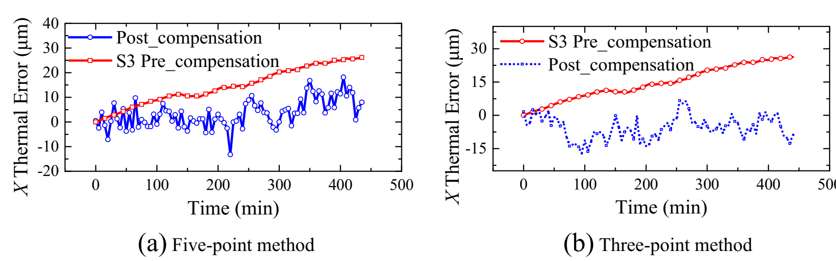

Fig. 15 Radial thermal error compensation in the X direction

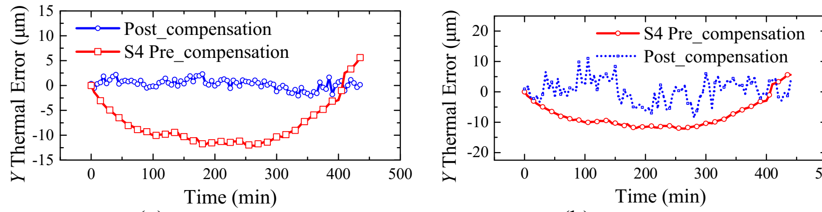

(a) Five-point method (b) Three-point method

Fig. 16 Radial thermal error compensation in the *Y* direction

method. So the five-point method is better than three-point method.

Characteristics of the CNC system determine that the spindle thermal error compensation can only be conducted at the end of its coordinates. And defects of the three-point method to measure the thermal drifts are as follows:

1. Due to the installation problem and other factors, the thermal deformation of the spindle terminal position is not easy to be directly measured by the displacement sensors. Generally speaking, the sensors are not assembled at the end of the spindle. Therefore, the measurement results do not accurately reflect thermal drifts of the end on the spindle, making a rough compensation model. While the distance between the end of the tool and the displacement sensor increases, the effect of the compensation based on the three-point method will be worse. Although the five-point method cannot measure the end thermal drifts also, the thermal error model proposed in this paper can calculate the compensated amounts of thermal offsets of the tool end, achieving a more accurate compensation.
2. Based on the three-point method, if the length of the cutting tool is changed, the thermal error model is no longer applicable because the influence of the tool length is ignored, and extra experiments are needed to establish a new model, which needs for better cost. While the compensation model of the thermal error does not need to be modified and has a perfect generalization based on the five-point method, considering the length of the cutting tools. In summary, the five-point method is better than the three-point method.

When the thermal offsets of the spindle are compensated on three directions based on the five-point method, the thermal inclination angle errors were reduced, and the result is shown in Fig. 17. After compensation, the maximum measurement of the thermal yaw angle error is 5″, and the average of the absolute value of the residuals is 1.2″. While the maximum thermal pitch angle error is 4.5″, the average of the absolute value of the residuals is 1.4″. In fact, the thermal inclination angle errors of the spindle system are not reduced, but by performing the thermal error compensation, the feed system moves the extra distances in the opposite direction of the thermal offsets. After compensation, the measured values of the thermal offsets reduced. And the θ_x and θ_y decreased calculated by Eqs. (12) and (13); therefore, the proposed method of the thermal error compensation can improve the terminal machining accuracy of the CNC machine tool.

5 Conclusions

Spindle thermal error modeling with axial elongation and radial thermal angle errors are suitable for actual practical conditions. This is due to the fact that it accurately describes thermal deformation space-pose and can consequently be used to improve machining accuracy. Radial thermal-induced angle errors were ignored in methods discussed in literature as most

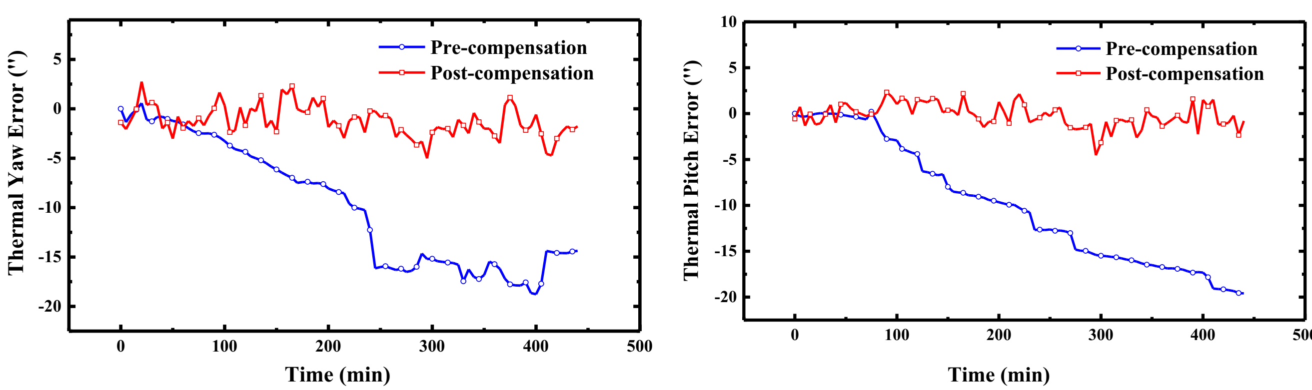

Fig. 17 Radial thermal angle errors compensation based on five-point method

methods are based on three-point measurement of the spindle thermal errors. To solve this problem, a five-point method was applied to measure the spindle thermal drifts. The use of a least square support vector machine model to incorporate thermal elongation and declination angles was proposed. The methods were based on fuzzy cluster with a high predictive accuracy. Moreover, the method combining fuzzy cluster and correlation analysis was proposed to group and optimize the temperature variables, reducing the multicollinearity of the temperature variables and the improving stability of the model. In addition, equations for thermal error offset were derived, which take into account the tilt angles and length of the cutting tools. As a result a real-time compensation was implemented. Experimental results demonstrate that the axial (in the X and Y directions) and radial accuracy were improved by 82.6, 66, and 90 %, respectively, which demonstrated that the proposed method of measurement, modeling, and compensation was effective.

Acknowledgments This research is supported by the National High-Tech R&D Program of China (863 Program) under Grant Number 2012AA040701.

Conflict of interest We declare that we have no financial and personal relationships with other people or organizations that can inappropriately influence our work; there is no professional or other personal interest of any nature or kind in any product or company that could be construed as influencing the position presented in, or the review of, the manuscript.

References

1. Bryan JB (1990) International status of thermal error research. CIRP Ann 39(2):645–656
2. Donmez MA, Hahn MH, Soons JA (2007) A novel cooling system to reduce thermally-induced errors of machine tools. CIRP Ann 56(1): 521–524
3. Jenq SC, Wei YH (2003) Characterizations and models for the thermal growth of a motorized high speed spindle. Int J Mach Tools Manuf 43(11):1163–1170
4. Creighton E, Honegger A, Tulsian A, Mukhopadhyay D (2010) Analysis of thermal errors in a high-speed micro-milling spindle. Int J Mach Tools Manuf 50(4):386–393
5. Zhao HT, Yang JG, Shen JH (2007) Simulation of thermal behavior of a CNC machine tool spindle. Int J Mach Tools Manuf 47(6):1003–1010
6. Yang S, Yuan J, Ni J (1996) The improvement of thermal error modeling and compensation on machine tools by CMAC neural network. Int J Mach Tools Manuf 36(4):527–537
7. Ouafi AE, Guillot M, Barka N (2013) An integrated modeling approach for ANN-based real-time thermal error compensation on a CNC turning center. Adv Mater Res Environ Mater Eng 664:907–915
8. Zhang Y, Yang JG, Jiang H (2012) Machine tool thermal error modeling and prediction by grey neural network. Int J Adv Manuf Technol 59(9–12):1065–1072
9. Vissiere A, Noutra H, Damak M, Gibaru O, David JM (2012) A newly conceived cylinder measuring machine and methods that eliminate the spindle errors. Meas Sci Technol 23(9):1–11
10. Vyroubal J (2012) Compensation of machine tool thermal deformation in spindle axis direction based on decomposition method. Precis Eng 36(1):121–127
11. Hong C, Ibaraki S (2012) Observation of thermal influence on error motions of rotary axes on a five-axis machine tool by static R-test. Int J Autom Technol 6(2):196–204
12. Huang YQ, Zhang J, Li X, Tian LJ (2014) Thermal error modeling by integrating GA and BP algorithms for the high-speed spindle. Int J Adv Manuf Technol 71(9–12):1669–1675
13. Wang HT, Wang LP, Li TM, Han J (2013) Thermal sensor selection for the thermal error modeling of machine tool based on the fuzzy clustering method. Int J Adv Manuf Technol 69(1–4):121–126
14. Yan JY, Yang JG (2009) Application of synthetic grey correlation theory on thermal point optimization for machine tool thermal error compensation. Int J Adv Manuf Technol 43(11–12):1124–1132
15. Zhang Y, Yang JG, Xiang ST, Xiao HX (2013) Volumetric error modeling and compensation considering thermal effect on five-axis machine tools. Proc Inst Mech Eng C J Mech Eng Sci 227(5):1102–1115
16. Fu YQ, Gao WG, Yang JY, Zhang Q, Zhang DW (2014) Thermal error measurement, modeling and compensation for motorized spindle and the research on compensation effect validation. Adv Mater Res Eng Solutions Manuf Proces IV 889–890:1003–1008
17. Miao EM, Gong YY, Niu PC, Ji CZ, Chen HD (2013) Robustness of thermal error compensation modeling models of CNC machine tools. Int J Adv Manuf Technol 69(9–12):2593–2603
18. Wu CW, Tang CH, Chang CF, Shiao YS (2012) Thermal error compensation method for machine center. Int J Adv Manuf Technol 59(5–8):681–689
19. Li Y, Zhao WH (2012) Axial thermal error compensation method for the spindle of a precision horizontal machining center. IEEE International Conference on Mechatronics and Automation, ICMA, 2319–2323
20. Pajor M, Zapata J (2013) Supervising and compensation of thermal error of CNC feed ball screw. Diagnostyka 14(2):37–42
21. Liu YL, LuY GD, Hao ZP (2013) Thermally induced volumetric error modeling based on thermal drift and its compensation in Z-axis. Int J Adv Manuf Technol 69(9–12):2735–2745
22. Gebhardt M, Mavr J, Furrer N, Widmer T, Weikert S, Knapp W (2014) High precision grey-box model for compensation of thermal errors on five-axis machines. CIRP Ann Manuf Technol 63(1):509–512
23. Wang W, Yang JG (2013) A combined error model for thermal error compensation of machine tools. Adv Mater Res Metal Mater Manuf Technol 820:147–150
24. Lin WQ, Xu YZ, Fu JZ, Chen ZC (2006) Thermal error modeling and compensation of spindles based on LS-SVM. International technology and innovation conference 2006. IET Conf Publ 524:841–846
25. Zhao CL, Wang YQ, Guan XS (2009) The thermal error prediction of NC machine tool based on LS-SVM and grey theory. Appl Mech Mater e-Eng Digit Enterp Technol VII 16–19:410–414
26. Leahy R, Wu Z (1993) An optional graph theoretic approach to data clustering: theory and its application to image segmentation. IEEE Trans PAMI 15(11):1101–1113
27. Han J, Wang LP, Cheng NB, Wang HT (2012) Thermal error modeling of machine tool based on fuzzy c-means cluster analysis and minimal-resource allocating networks. Int J Adv Manuf Technol 60(5–8):463–472
28. Vapnik VN (1998) Statistical learning theory. Wiley, New York
29. Suykens JA, De BJ, Lukas L, Vandewalle J (2002) Weighted least squares support vector machines: robustness and sparse approximation. Neurocomputing 48(1):85–105
30. ISO 230–3 (2007) Test code for machine tools part 3: determination of thermal effects. ISO copyright office, Switzerland